Biomedicine & Pharmacotherapy 146 (2022) 112596

Contents lists available at ScienceDirect

Biomedicine & Pharmacotherapy

journal homepage: www.elsevier.com/locate/biopha

MiR-125b downregulates macrophage scavenger receptor type B1 and reverse cholesterol transport

Miguel Hueso [a,b,*], Raquel Griñán [c,d], Adrián Mallen [b], Estanislao Navarro [b], Elvira Purqueras [e], Montse Gomá [e], Fabrizio Sbraga [f], Arnau Blasco-Lucas [f], Giovanna Revilla [c], David Santos [g], Marina Canyelles [c], Josep Julve [c,g], Joan Carles Escolà-Gil [c,g,**], Noemi Rotllan [c,g,**]

[a] Department of Nephrology, Hospital Universitari Bellvitge and Bellvitge Research Institute (IDIBELL), L'Hospitalet de Llobregat, 08907 Barcelona, Spain
[b] Nephrology and Renal Transplantation Group, Infectious Disease and Transplantation Program, Institut d'Investigació Biomèdica de Bellvitge-IDIBELL, L'Hospitalet de Llobregat, 08907 Barcelona, Spain
[c] Institut d'Investigacions Biomèdiques (IIB) Sant Pau, C/ Sant Quintí 77, 08041 Barcelona, Spain
[d] Departament de Bioquímica i Biologia Molecular, Universitat Autònoma De Barcelonna, 08041 Barcelona, Spain
[e] Department of Pathology, Hospital Universitari Bellvitge and Bellvitge Research Institute (IDIBELL), L'Hospitalet de Llobregat, 08907 Barcelona, Spain
[f] Department of Cardiac Surgery, Hospital Universitari Bellvitge and Bellvitge Research Institute (IDIBELL), L'Hospitalet de Llobregat, 08907 Barcelona, Spain
[g] CIBER de Diabetes y Enfermedades Metabólicas Asociadas (CIBERDEM), Barcelona, Spain

ARTICLE INFO

Keywords:
Cholesterol efflux
Reverse cholesterol transport
Scavenger receptor class B type 1 (SRB1)
MicroRNA
MiR-125b
Macrophage
Vascular smooth muscle cell
Coronary artery disease

ABSTRACT

Objective: To determine whether miR-125b regulates cholesterol efflux *in vivo and in vitro through the regulation of scavenger receptor type B1 (SR-B1).*
Approach and results: We demonstrated that miR-125b is up-regulated in the human aortas of patients with CAD and is located in macrophages and vascular smooth muscle cells (VSMCs). We identified *SCARB1* as a direct target of miR-125b by repressing the activity of the *SCARB1* 3′-untranslated region reporter construct. Moreover, the overexpression of miR-125b in both human and mouse macrophages as well as VSMCs was found to downregulated the expression of the *SCARB1* and the SR-B1 protein levels, thereby impairing α-HDL-mediated macrophage cholesterol efflux *in vitro*. The *in vivo* reverse cholesterol transport (RCT) rate from non-cholesterol-loaded macrophages transfected with miR-125b to feces was also found to be decreased when compared with that of control mimic-transfected macrophages.
Conclusions: Together, these results provide evidence that miR-125b downregulates *SCARB1* and SR-B1 in both human and mouse macrophages as well as VSMCs, thereby impairing macrophage cholesterol efflux *in vitro* and the whole macrophage-specific RCT pathway *in vivo*.

1. Introduction

The accumulation of macrophages in the artery wall, and the subsequent foam cells formation are hallmarks of vascular lesions in atherosclerosis (ATH) progression. Since macrophages do not express pathways for catabolizing cholesterol, the ability of high-density lipoproteins (HDL) particles to stimulate the efflux of excess free cholesterol is critical in reducing foam cell formation [1]. Macrophage cholesterol efflux occurs *via* several pathways, one of these pathways is called passive diffusion, and it may be facilitated by scavenger receptor class B type 1 (SR-B1), and the other pathways are active processes involving the ATP-binding cassette (ABC) A1 and G1 transporters [2]. SR-B1 is widely expressed throughout the different cell types and both preclinical experimental and clinical studies have shown that the disruption of SR-B1 function predisposes to the development of ATH and cardiovascular disease [3,4], although there is a controversy in different human

Abbreviations: ABCA-1, ATP-binding cassette transporter A1; ATH, atherosclerosis; BOECS, Blood Outgrowth Endothelial Cells; CAD, coronary artery disease; ECs, Endothelial Cells; HDL, high-density lipoprotein; miRNA, microRNA; RCT, reverse cholesterol transport; SCARB1, scavenger receptor class B type 1 gene; SR-B1, scavenger receptor class B type 1; 3′UTR, 3′ untranslated region; VSMCs, Vascular smooth muscle cells; WT, Wild-type.

* Correspondence to: L'Hospitalet de Llobregat, 08907 Barcelona, Spain.
** Correspondence to: C/ Sant Quintí 77, 08041 Barcelona, Spain.
E-mail addresses: mhueso@idibell.cat (M. Hueso), JEscola@santpau.cat (J.C. Escolà-Gil), nrotllanv@santpau.cat (N. Rotllan).

https://doi.org/10.1016/j.biopha.2021.112596
Received 29 September 2021; Received in revised form 16 December 2021; Accepted 23 December 2021
Available online 28 December 2021

genetic studies with rare SCARB1 mutations and the association with CAD and levels of HDL cholesterol (HDL-C) [5–7]. Interestingly, the contribution of macrophage SR-B1 to the pathogenesis of ATH appears to be highly dependent on the foam cell formation stage [3]. In addition, other cell types, such endothelial (ECs) and vascular smooth muscle cells (VSMCs) can also become foam cells [8,9], although the contribution of SR-BI-mediated cholesterol efflux pathways on foam cell formation in these particular cell types remains unknown.

Small non-coding miR-125b was associated with ATH development in an experimental model, and it was also found to be upregulated in human atherosclerotic plaques of abdominal aortas from deceased patients [10]. Furthermore, the relative abundance of miR-125b was found to be up-regulated by the CD40-NF-κB signaling axis in activated mouse macrophages [10]. Also, a microRNA expression quantitative trait loci-mapping study of whole blood from a large cohort identified the polymorphisms of cis-acting regulatory elements of miR-125b highly associated with HDL-C [11]. In this context, miR-Base screening detected that the 3′-untranslated region (3′-UTR) from the *SCARB1* gene, which encodes SR-B1, was a predicted target for miR-125a and miR-125b [12]. This latter study also reported that miR-125a down-regulated SR-B1 expression by direct targeting and inhibiting SR-B1-mediated selective HDL uptake in mouse and rat steroidogenic cells [12].

Since SR-B1 is highly expressed in foam cells within human aortic ATH [13], here, we aimed to evaluate the role of miR-125b in regulating SR-B1-mediated macrophage as well as VSMCs cholesterol efflux to HDL particles *in vitro* and the entire macrophage-specific reverse cholesterol transport (RCT) pathway *in vivo*.

2. Materials and methods

The data, analytical methods, and study materials that support the findings of this study will be available to other researchers upon reasonable request. A detailed research materials is listed in the online Supplemental materials.

2.1. Patients and histology

This study analyzed blood and samples from ascendant aortas obtained in the surgery scenario. Samples and data from the patients included in this study were provided by the Biobank HUB-ICO-IDIBELL (PT17/0015/0024), which is integrated within the Spanish National Biobanks Network. The study was approved by the ethics committee of Bellvitge University Hospital (PR149/14, approved on May 19th, 2016) and all participants provided their written informed consent. The demographic characteristics have been previously published [14].

2.2. Histology and in situ hybridization

The human aorta samples were fixed in 10% neutral buffered formalin for two days, followed by one day in 15% sucrose. The typical protocol for embedded tissues in paraffin was performed as well as that for hematoxylin-eosin (HE) staining. For antagomir fluorescence *in situ* hybridization (AISH), fresh-frozen human aorta samples were fixed in 4% paraformaldehyde (PFA) and embedded in OCT. Tissue sections of 8 μm were cut by using a microtome-cryostat and stored on SuperFrost slides at − 80 °C until the AISH was performed. The cryosections were thawed 10 min at room temperature (RT), dried for 10 min at 50°C, and then fixed in 4% PFA for 10 min followed by two washes with DEPC-treated 1 × PBS at RT for 3 min in a Coplin jar with agitation. An *in situ* hybridization assay was performed as previously described [15]. Briefly, 5′-fluorescein Cy5 probes (25 nM AntagomiR-125b or 25 nM AntagomiR Cel-miR-67 scrambled control provided by Dharmacon) were added to 10 μL of IQFISH Hybridization Buffer. The probe mixture was added to the tissue sample and covered with a coverslip, incubated on the hybridizer for 90 min at 70 °C (temperature was adjusted considering the predictive Tm values of the probe used). After the hybridization incubation, the coverslips were removed and the slides were washed three times in a Coplin jar with 0.01 × SSC at 78 °C (4–8 °C above the hybridization temperature) with 10 min per wash in agitation. Then, the slides were switched to a Coplin jar with 2 × SSC at RT and incubated for 5 min with agitation. The tissue slides were dried for 5 min at RT, embedded with a DAPI mounting medium, and covered with a glass coverslip to keep the slides at 4 °C under dark conditions until microscope imaging. Fluorescence imaging was performed using a Carl Zeiss LSM880 spectral confocal microscope. We used a 63 × objective with NA of 1.4. For the excitation of the DAPI, we used 405 nm-laser line, and for Cy5, we used a 633 nm-laser line. The images were analyzed with Zen Black 2.3 Software.

2.3. Immunohistochemistry

Consecutive sections to the AISH aortas were cut into of 8 μm-thick sections on a cryostat and placed on a Ventana Ultra View Autostainer. The sections were dried at 95 °C for 8 min. The slides were pretreated at 95 °C for heat-induced antigen retrieval in a Tris_EDTA Cell Conditioning Buffer (CC1) (pH = 8.4) for 64 min followed by incubation with the ready-to-use mouse monoclonal antibody, CONFIRM™ anti-CD68 (KP-1) Primary Antibody (Ventana Medical Systems, Arizona, USA), at 37 °C for 32 min, or alpha smooth muscle actin (GA61161-2, Agilent Technologies, Inc., Glostrup, Denmark) at 37 °C for 20 min. Next, the slides were counterstained with hematoxylin for 12 min and a bluing reagent for 4 min.

2.4. Cell culture and miRNA mimic transfections

Human monocytic (THP-1) and mouse macrophages (J774A.1 and RAW264.7) as well as mouse vascular smooth muscle (VSMC, CRL-2797) cells were obtained from American Type Tissue Collection (ATTC).CHO (Chinese-hamster ovary) cells were kindly provided by Dr. Joerg Heere. The THP-1 cells were maintained in RPMI 1640 media supplemented with 10% fetal bovine serum (FBS) (Pan Biotech, Aidenbach, DE) and 1% penicillin-streptomycin (Dominique Dutscher, Brumath, France) at 37 ºC and 5% CO_2. THP-1 differentiation into macrophages was induced using 50 ng/mL PMA for 24 h. The J774A.1 cells were maintained in Dulbecco's Modified Eagle Medium (DMEM) supplemented with 10% FBS and 1% penicillin-streptomycin. The VSMCs were maintained in DMEM supplemented with 10%FBS and 0.2% G418 antibiotic. The CHO cells were maintained in F-12 media (HAM) supplemented with 10% FBS and 1% penicillin-streptomycin. The THP-1 and J774A.1 macrophages, along with the VSMCs were seeded at a density of 1.5×10^6, 1×10^6, and 2×10^5 cells per 6-well plates, respectively, and transfected the following day with 40 nM of control mimic (CM) or hsa-miR-125b-5p mimic (miR-125b) for 48 h utilizing the RNAimax Transfection Reagent (Invitrogen, Carlsbad, CA) according to previously established protocols [16].

Human aortic cell and blood outgrowth endothelial cells (BOEC) isolation and culturing are detailed in the on line Supplemental materials.

2.5. Dual luciferase assays

In order to determine whether SCARB-1 3′UTR activity is regulated by miR-125b, RAW264.7 cells (2×10^5 cells/well) were seeded separately in 96-well opaque plates (#6005660; PerkinElmer, Massachusetts, USA) overnight to reach 80–90% confluence. Twenty-four hours after seeding, the cells were transfected with 100 ng pMirTarget reporter constructs, both p_SCARB1. WT with the wild type 3′UTR region of SCARB1 (#SC211509; Origene pSCARB1–3′UTR SCARB1 (NM_005505) Human 3′UTR Clone) and p_SCARB1. Mut with the mutated miR-125b predicted binding site from SCARB1 3′UTR (#SC211509_CW306882 Origene Technologies, Maryland USA) alone as reference controls or

together with 40 nM mirVana hsa-miR-125b-5p miRNa mimic (#4464066-MC10148; Thermofisher Scientifics, Massachusetts USA) using 0.3 μL TransIT-X2 (#6004 MirusBio, Wisconsin USA) according to the manufacturer's protocol. Forty-eight hours after transfection, when the cells reached the desired 100% confluence, the luminescence activity was measured using the Luciferase Assay System (#E4530; Promega, Wisconsin USA). Briefly, the cells were lysed with 20 μL 1 × Reporter Lysis Buffer. Then, the RFP fluorescence signal of the cells was measured with a FLUOstar OPTIMA Plate Reader (BMG LabTech) at Ex 530 nm and Em 620 nm. Next, 100 μL of Luciferase Assay Reagent was added to each lysate, and the luminescence signal was immediately measured with the FLUOstar OPTIMA Plate Reader (BMG LabTech). All samples were measured in triplicate. For further evaluation, the luminescence values were normalized to the RFP values, and the miR-125b mimic values were normalized to the p_SCARB1 controls.

2.6. In vitro cholesterol efflux radioactivity assays

HDL (1.063–1.210 g/mL) was isolated from the normolipidemic plasma *via* sequential ultracentrifugation (using potassium bromide for density adjustment) at 100,000 × *g* for 24 h with an analytical fixed-angle rotor (50.3, Beckman Coulter, Fullerton, CA, USA). The cellular cholesterol efflux was determined after seeding the 1×10^6 human THP-1 and 0.5×10^6 mouse J774A.1 macrophage, as well as the 0.2×10^6 mouse VSMC, respectively, per well in 6-well plates; these were allowed to grow for 24 h in a complete RPMI 1640 medium containing 2 mmol/L L-glutamine (Pan Biotech, Aidenbach, DE) supplemented with 10% FBS and 100 U/mL penicillin/streptomycine. At that time point, the cells were transfected with 40 nM of CM or miR-125b for 48 h. Then, the cells were labeled for 24 h in the presence of 1 μCi/well of [1α,2α(n)-^{3}H] cholesterol (Perkin Elmer, Boston, MA, USA) and 5% FBS, as previously reported [17]. The cells were then equilibrated with 0.2% bovine serum albumin (Sigma-Aldrich) in the medium for 1 h and incubated for 4 h with the total HDL (25 μg/mL of APOA1) in the free medium. The radioactivity was then measured in both the medium and the cells, and the percentage of cholesterol efflux was calculated [17]. This experiment was also performed after incubating purified APOA1 (25 μg/mL) with macrophages after stimulating the ABCA1-dependent efflux pathway by treating the cells with 0.3 mmol/L 8-(4-Chlorophenylthio) adenosine 3′,5′-cyclic monophosphate (pCPT-cAMP, Sigma-Aldrich) during the equilibration period.

2.7. In vitro cholesterol efflux fluorescent assay

The *in vitro* cellular cholesterol efflux was also determined using TopFluor-cholesterol, a fluorescent cholesterol probe in which the cholesterol molecule is linked to a boron dipyrromethene difluoride (BODIPY) moiety (Avanti Polar Lipids, Alabaster, AL, USA). The J774A.1 cells (1×10^5/well) were seeded in 48-well plates and allowed to grow for 24 h in a DMEM-supplemented medium. The cells were transfected with CM or miR-125b for 48 h as previously explained in Section 2.4. Next, the macrophages were labeled for 1 h in a high-glucose DMEM medium (Lonza, Waltham, MA, USA) containing 0.125 mmol/L total cholesterol, where the fluorescent cholesterol accounted for 20% of the total cholesterol complexed with 10 mmol/L methyl-β-cyclodextrin (Sigma-Aldrich, Madrid, Spain), as reported previously [18]. The labeled cells were subsequently equilibrated for 18 h with DMEM containing 0.2% fatty-acid free BSA (Sigma-Aldrich, Madrid, Spain) and then incubated for 24 h with the total HDL (25 μg/mL of APOA1) in the free medium. The fluorescence intensity was then measured in the medium using the microplate reader, Synergy HT (BioTek Instruments, Winooski, VT, USA), at λEx/Em = 485/530 nm. The cells were solubilized with 1% cholic acid and mixed on a plate shaker for 4 h at room temperature, and the fluorescence intensity was quantified. The cholesterol efflux capacity was calculated according to the formula: [media fluorescence/(media fluorescence + cells fluorescence)] × 100.

2.8. In vitro cholesterol influx assay

Radiolabeled lipoproteins were prepared in a manner adapted from the method developed by Cedo et al. [19]. First, 5 μCi of [1α,2α(n)-^{3}H] cholesterol (Perkin Elmer) was mixed with absolute ethanol, and the solvent was evaporated under a stream of N_2. The total HDL was added to the [1α,2α(n)-^{3}H]cholesterol-containing tubes (0.5 mL, 2.11 mg/mL of apoAI) and then incubated for 4 h in a 37 °C bath. The labeled HDL was reisolated by ultracentrifugation at 1.063–1.210 g/mL and dialyzed against PBS *via* gel filtration chromatography. Cells were incubated with 25 μg of HDL for 4 h in a free medium. The percentage of cholesterol infflux was calculated by measuring the radioactivity in the cells after adding 0.2 N NaOH [17].

2.9. In vivo macrophage-specific reverse cholesterol transport

All animal procedures were conducted in accordance with the published regulations and reviewed and approved by the Institutional Animal Care Committee of the Institut de Recerca of the Hospital de la Santa Creu i Sant Pau (ref. 10626). We used 24-week-old male C57BL/6 mice fed with a Western-type diet (TD.88137, Envigo, Indianapolis, IN, USA) containing 21% fat and 0.2% cholesterol for four weeks. The mouse J774A.1 macrophages were cultured in 75 cm^2-tissue culture plates in a RPMI-supplemented medium. The cells were then transfected with 40 nM of CM or miR-125b for 48 h. After that, the cells were incubated for 24 h in the presence of 5 μCi/mL of [1α,2α(n)-^{3}H]cholesterol and 10% inactivated human lipoprotein-depleted serum (LPDS). These cells were washed, equilibrated with a medium containing 0.2% bovine serum albumin, detached *via* scraping, resuspended in PBS, and pooled before being intraperitoneally (i.p.) injected into the mice (2.76×10^6 macrophages transfected with CM and containing 4.53×10^6 cpm per mouse; and 3.05×10^6 macrophages transfected with miR-125 and containing 4.62×10^6 cpm per mouse); the cell viability was 85% in both macrophages, as measured *via* trypan blue staining [17]. The mice were then individually housed, and their stools were collected over the next 48 h. Serum radioactivity was determined *via* liquid scintillation counting. The [^{3}H] HDL-cholesterol levels were measured in plasma obtained after the precipitation of APOB-containing lipoprotein particles. Liver and fecal lipids were extracted with isopropyl alcohol-hexane (2:3, v:v) and the [^{3}H]tracer detected in the cholesterol and fecal bile acids was determined as previously described [19].

2.10. RNA isolation and quantitative real-time PCR

The total RNA was isolated from the cells using TRIzol Reagent (Invitrogen, Carlsbad, CA) according to the manufacturers protocol and purified using the EZ-10 DNAaway RNA Miniprep Kit (Bio Basic, Markham, Canada). One microgram of total RNA was reverse-transcribed using EasyScript First-Strand cDNA Synthesis SuperMix (Transgen Biotech, Beijing, China) following the manufacture's protocol. Quantitative real-time PCR amplification was performed in duplicates using the GoTaq(R) Probe qPCR Master Mix (Promega, Madison, WI). Specific TaqMan probes (Applied Biosystems, Foster City, CA) were used for human SCARB1 (Hs00969827_m1) and mouse Scarb1 (Mm00450236_m1); for human ABCG1 (Hs00245154_m1) and mouse Abcg1 (Mm00437390_m1); and human (Hs03928985_G1) or mouse Rn18s rRNA (Mm03928990_g1) were used as internal control genes. The reactions were run on a the CFX96TM Real-Time System (Bio-Rad, Hercules, CA, USA). The relative mRNA expression levels were calculated using the ΔΔCt method. The mRNA levels were normalized to 18S rRNA.

2.11. miRNA quantification

For miRNA quantification, TaqMan mature miRNA detection kits were used. Primers specific for human and mouse miR-125b (hsa-miR-125b-5p, assay ID 002198, TaqMan microRNA Assays, ThermoFisher Scientifics, MA USA) were used for cDNA production and qRT-PCR analysis and normalized to U6 as a housekeeping gene. The miR-125b quantification and quantitative real-time PCR were performed in duplicate using TaqMan RT mix on an iCycler real-time detection system (Eppendorf).

2.12. Western blot analysis

The human THP-1 and mouse J774.1macrophages as well as the VSMC cells were lysed in ice-cold buffer containing 50 mM Tris–HCl, pH 7.5, 0.1% SDS, 0.1% deoxycholic acid, 0.1 mM EDTA, 0.1 mM EGTA, 1% NP-40, 5.3 mM NaF, 1.5 mM NaP, a 1 mM orthovanadate and 1 mg/mL of protease inhibitor cocktail (Roche Diagnostics, Basel, Switzerland), and 0.25 mg/mL AEBSF (Roche). Cell lysates were centrifuged at 12,000 *g* for 15 min at 4 °C, and the protein concentrations of the supernatants were determined using the BCA Protein Assay Reagent Kit (A53227, Thermo Scientific, Waltham, MA, USA). The protein extracts were mixed with a corresponding volume of 4 × Laemmli loading buffer containing 62.5 mM Tris-HCl pH 6.8, 2% SDS, 25% glycerol, and 0.01% bromophenol blue and heated at 94 ºC for 4 min. Then, 20 µg of total protein from each sample was separated onto a 7.5% TGX Stain Free PreCast Gel (4568026, Bio-Rad, Carson, CA, USA) and transferred to a 0.22 µm PVDF membrane (1704157, Bio-Rad, Carson, CA, USA). Nonspecific sites on the membrane were blocked with either 3% dried milk in Tris-buffered saline containing 0.05% Tween-20 (TBST buffer) for 15 min. Membranes were incubated overnight at 4 ºC with optimized dilutions of the primary antibody SCARB1 (Abcam 36970, Cambridge, UK), of 1:1000 or, for ABCG1 (Novus Biologicals, Centennial, CO, NB400-132SS), of 1:500. The following day, the membranes were washed with the TBST buffer and reincubated with IgG HRP-conjugated anti-rabbit secondary antibody (W401B, Promega, Madison, USA) for 1 h. After that, the membranes were washed with the TBST buffer and revealed using the Immun-Star WesternC Chemiluminescence Kit (170-5070, Bio-Rad, Carson, CA). Imaging and data analysis: TGX Stain-Free gels were activated for 1 min after SDS–electrophoresis, and images were captured using ChemiDOC™XRS Gel Documentation Systems (Bio-Rad, Hercules, CA) and ImageLab software (version 6.0.1, Bio-Rad, Richmond, CA). Data normalization analysis was performed using the stain free images. The approximate molecular weights of the target proteins were determined *via* comparison with a prestained protein ladder (ab116028, abcam, Cambridge, UK).

2.13. Statistical analysis

The *in vitro* experiments were routinely repeated at least three times (with three replicates per experiment) unless otherwise noted. The data is presented as the mean ± SEM (n is noted in the figure legends). D′Agostino & Pearson and Shapiro-Wilk normality tests were performed to identify Gaussian distributions. When the data followed a Gaussian distribution, Student's *t*-test was used to compare the differences between two groups. The number of mice per group was estimated considering $\alpha = 0.05$, power = 80%, and an effect size of 0.5% in the fecal excretion of the macrophage-derived tracer. The subjects were randomized into groups and all animals were included in the analyzes. The experiments were conducted blinded regarding the origin of the specimens in order to reduce bias. Significance was accepted at the level of $p < 0.05$. GraphPad Prism version 8.0 for Windows (GraphPad Software, San Diego, CA) was used to perform all statistical analyses.

3. Results

3.1. Hsa-miR-125b expressed in the macrophages and VSMCs of the arteries obtained from patients with CAD and targeted the 3′-UTR of SCARB1 mRNA

We previously reported the upregulation of hsa-miR-125b in atherosclerotic plaques from abdominal aortas obtained from deceased patients [10]. Here, we first validated these results in a second independent cohort of patients with CAD by testing the hsa-miR-125b expression in ascendant aortas collected in the surgery scenario (representative histological sections from those aortas can be found in Fig. IA–B in the online Supplemental materials). As shown in Fig. 1A, hsa-miR-125b was up-regulated, confirming that miR-125b may actually be activated during ATH progression. We next aimed to identify which cells were overexpressing hsa-miR-125b in the vascular lesions by performing *in situ* hybridization for hsa-miR-125b in three independent aorta samples from ascendant aortas obtained during cardiac surgery (Fig. 1B–C). We found that hsa-miR-125b was predominantly expressed in macrophages (Fig. 1B–C) and VSMCs (Fig. 1C). More detailed images of a single Z-section of monocytes labeled with a Cy5-conjugated anti-hsa-miR-125b antagomir in a vasa vasorum from the aortic adventitia are shown in Fig. 1B. To confirm that the cells were monocytes, staining of the correlative section was performed with anti-CD68 antibody (Fig. 1B). We also analyzed the expression of miR-125b in BOECs and ECs; miR-125b was not expressed in these cells (data not shown).

Since macrophage cholesterol efflux is essential for homeostasis and critical in ATH pathogenesis [2], we focused on these cells and we performed a bioinformatics analysis to identify potential hsa-miR-125b target genes related to cholesterol metabolism using the TargetScan v.7.2 data base. We detected that *SCARB1*, *LIMA1* (LIM Domain and Acting Binding 1, NCBI = 51474) and *VPS4B* (Vacuolar Protein Sorting 4B, NCBI = 9525) had predicted binding sites for hsa-miR-125b. Specifically, we focused on studying SCARB1, since its importance of *SCARB1* during cholesterol efflux is well known in addition to its dysfunction that predispose to the pathogenesis of ATH. The human *SCARB1* 3′UTR gene has only one computationally predicted miR-125b binding site in the second 3′UTR (Fig. 2A), and, for the murine *Scarb1* gene, there are three predicted miRNA binding sites in the three different 3′UTR variants (Fig. IIA–C in the online Supplemental materials). To directly assesses whether the hsa-miR-125b targets the 3′UTR of *SCARB1*, we transfected mouse macrophage cells with a reporter construct with the luciferase coding sequence fused to the 3′UTR of *SCARB1*. Interestingly, hsa-miR-125b markedly repressed the activity of the *SCARB*1 3′UTR reporter construct (Fig. 2B). Importantly, when we mutated the binding site of miR-125b in the 3′UTR of *SCARB1*, the luciferase activity increased (Fig. 2B), thereby providing direct evidence that miR-125b regulates *SCARB1 via* directly binding to *SCARB1*-3′UTR. Furthermore, we observed that miR-125b was inversely related to but — not significantly associated with—*SCARB1* expression in the ascendant aortas of the patients (Fig. 2C).

3.2. miR-125b downregulates macrophage SCARB1 and impairs HDL-mediated macrophage cholesterol efflux and macrophage-to-feces RCT in vivo

We next investigated the physiological role of miR-125b *in vitro* and *in vivo*. Specifically, in order to establish whether the increased expression of miR-125b in macrophages would directly regulate the expression of SCARB1 and α-HDL-mediated macrophage cholesterol efflux *in vitro,* we transfected human THP-1 monocyte–derived macrophages, J774A.1 mouse macrophages and VSMCs with miR-125b. Gene and protein expression analysis demonstrated that the overexpression of hsa-miR-125b significantly reduced the *SCARB1* mRNA and protein levels in the three cell types studied (Fig. 3A–C, left showing mRNA and

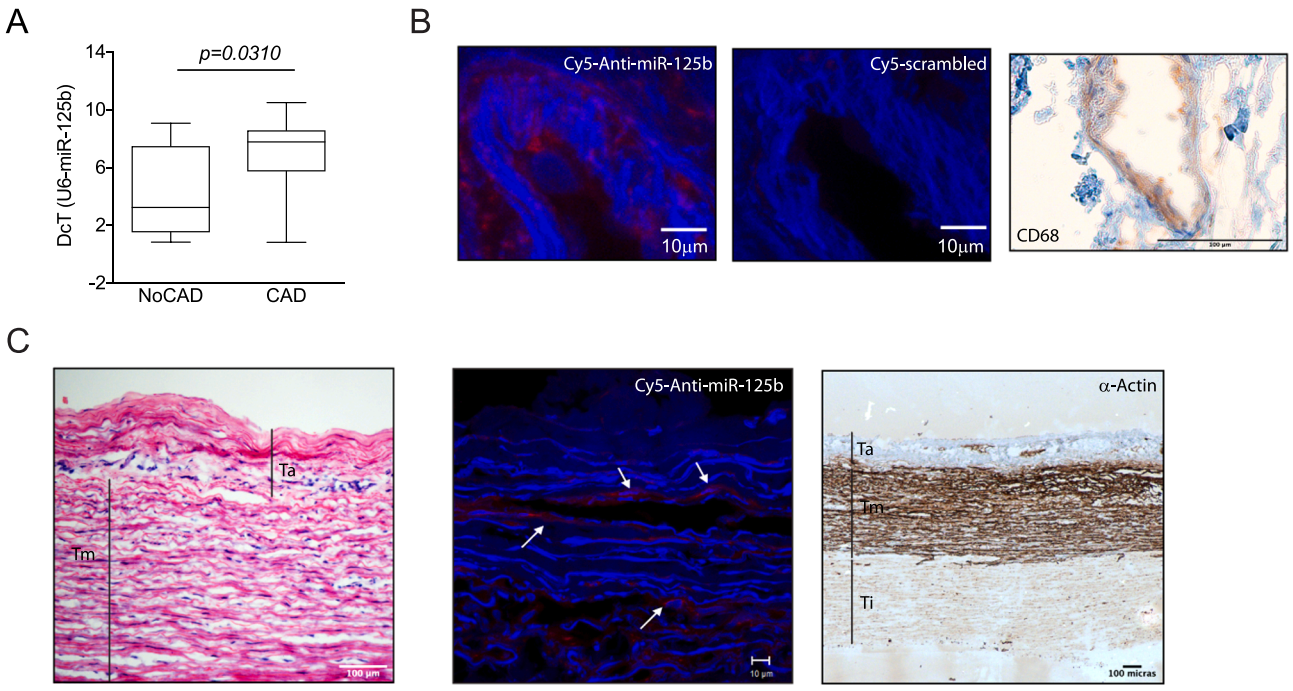

Fig. 1. Aortic miR-125b expression in patients with CAD and the regulation of miR-125b accessibility to the 3′UTRs of the different *scarb1* transcript variants. (A) Boxplot of hsa-miR-125b expression in the aortas of patients with CAD (n = 33) *vs* those without CAD (non-CAD) (n = 5). Hsa-miR-125b expression was normalized to U6 levels. (B) Representative *in situ* single Z-section of a vase from the vasa-vasorum of the aortic adventitia showing a monocyte adhered to ECs labeled with 25 mM of a Cy5-conjugated anti-miR-125b antagomir and their scrambled negative control (right image). Nuclei were stained in blue with 4,6-diamidino-2-phenylindole (DAPI), and miR-125b was stained in red with Cy5. Staining with anti-CD68 antibody reveal their monocyte origin. (C) Representative transverse histological sections from an ascending aortic wall of a patient with CAD and stained with H&E (left panel) where the *in situ* hybridization was performed (middle panel) and alpha-actin showing a diffuse intimal thickening characterized by an increase in fusiform cells (right panel). The black arrows indicate the tunica intima (Ti), tunica media (Tm), and tunica adventitia (Ta). Scale bars represents 100 μm. A fluorescent *in situ* hybridization (AISH) (middle panel) shows the localization of miR-125b in the cytoplasm of human monocyte (Mc) and VSMCs. The white arrows indicate positive cells for miR-125b. Scale bars represents 10 μm.

upper panel showing protein). However, miR-125b expression did not significantly affect the abcg1 mRNA and protein levels (Supplementary Fig. III in the online Supplemental materials). Also, we found very low levels of macrophage abca1 mRNA, and protein was not detected by western blot in these non-cholesterol-loaded cells. This reduction in SCARB1 mRNA and protein level was associated with an impaired macrophage radioactive cholesterol efflux to α-HDL (Fig. 3A–C, right). This was also confirmed *via* TopFluor-cholesterol efflux assay, where the cholesterol efflux in J774 cells transfected with CM was 19.40% *vs* 14.75% in cells transfected with miR-125b. Furthermore, the sole stimulation of ABCA1 by pCPT-cAMP did not affect the cholesterol efflux promoted by lipid-free ApoA1 (Fig. 3D). Importantly, the miR-125b expression did not affect the α-HDL-mediated cholesterol efflux from CHO cells expressing SCARB1, which does not contain the target SR-B1 3′-UTR sequence (Fig. 3E).

We also investigated the potential of miR-125b in regulating macrophage cholesterol influx. The total HDL was labeled and incubated with J774.1 macrophages after transfection with CM or miR-125b. The percentage of cholesterol influx was similar in the CM and miR-125b transfected cells (4.87% ± 0.18 *vs* 5.10% ± 0.24, respectively).

Next, we investigated the role of the macrophage expression of miR-125b in RCT *in vivo*. [^{3}H]cholesterol-labeled J774A.1 mouse macrophages transfected with CM or hsa-miR-125b were injected i.p. into wild-type C57BL/6 mice fed a Western-type diet for four weeks. The plasma [^{3}H]tracer levels in the mice injected with the hsa-miR-125b transfected macrophages were decreased at 4, 24 and 48 h after injection and these changes were mainly due to lower levels of HDL-associated [^{3}H]cholesterol (Fig. 4A–B). Importantly, the overall transfer of cholesterol from the miR-125b-transfected macrophages to the liver and feces was significantly impaired when compared to that of the CM-transfected macrophages (Fig. 4C–D).

4. Discussion

Our study was originally set up to deepen understanding of the mechanism by which miR-125b affects the pathogenesis of ATH. We previously detected that miR-125b was upregulated in a mouse model of ATH and in the abdominal aorta of deceased patients [10]. Here, in a second independent cohort, we validated this previous result, and, in the ascendant aortas of patients with ischemic heart disease, we detected that the expression of miR-125b was also highly up-regulated.

miR-125b has also been reported to be highly expressed in vascular murine ECs [20], and it was also physiologically expressed in murine steroidogenic cells, although at much lower levels than miR-125a, which targeted the *SCARB*1 gene and downregulated the SR-B1-mediated selective HDL cholesterol esters uptake [12]. However, human ECs and BOECs did not express miR-125b, rather indicating a differential expression of this miRNA across both species and cell types. Since vascular ECs and circulating BOECs from patients expressed *SCARB1* but not miR-125b, we focused our study on macrophages and VSMCs. Thus, our study extended on the regulating mechanism of miR-125b and predicted the miRNA binding sites of the 3′UTR *SCARB1* gene, which was validated *via* luciferase assays in macrophages. However, although hsa-miR-125b was inversely associated with *SCARB1* expression in the human aortas, this pattern did not reach statistical significance. It is possible that the aortic cell diversity and wide range of *SCARB1* expression in multiple cell types [3] could partly attenuate the inverse association between hsa-miR-125b and *SCARB1*, since *SCARB1* is expressed in ECs but not miR-125b.

We further determined whether the increased expression of hsa-miR-125b resulted in lower endogenous SR-BI expression levels and the altered cholesterol efflux in human and mouse macrophages, as well as VSMCs. Since the cholesterol-laden macrophages showed lower SR-BI

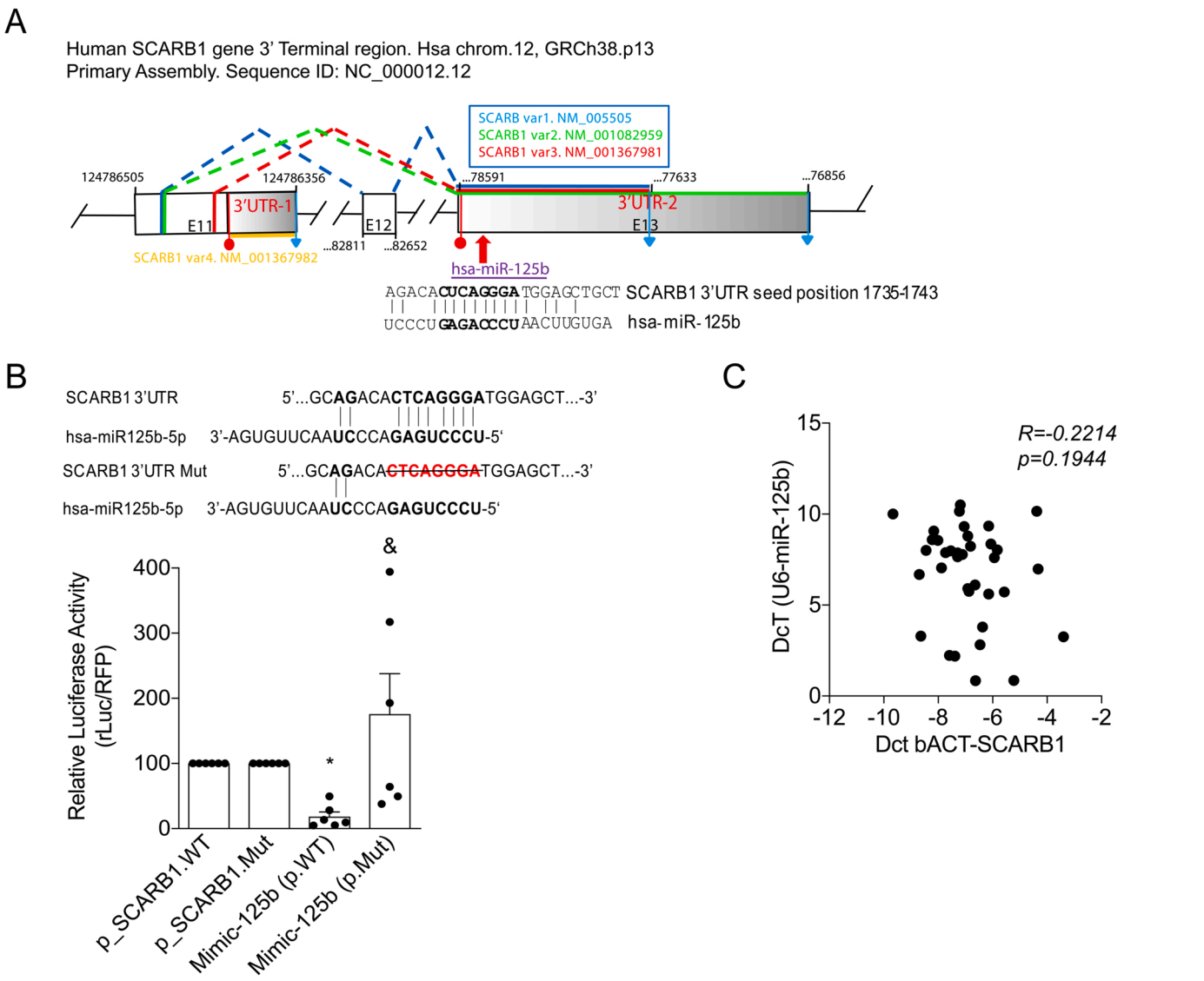

Fig. 2. Regulation of miR-125b accessibility to the 3′UTRs of the different *scarb1* transcript variants. (A) Structure of the 3′ terminal region of the human *SCARB1* gene. Boxes identify exons 11–13, the two UTRs, and their relative positions in the original genomic sequence (NC_000012.12). Interrupted black lines indicate intronic sequences. Splicing variants are color-coded. Colored doted lines linking the exons show alternative splicing events. Vertical colored bars in exon 11 show the cryptic splice sites predicted in this exon. Colored solid horizontal lines in both 3′UTRs show the lengths for each splicing variant of *SCARB1*. Red circles indicate the position of the functional stop-codons. Inverted blue triangles indicate the positions of the polyadenylation signals (PAS). Also shown is the binding site for hsa-miR-125b in the 3′UTR of *SCARB1* variant 1 (seed sequence in bold). This genomic map was drawn by blasting the following cDNA sequences—*SCARB1* variant 1 (NM_005505/ENST00000261693), *SCARB1* variant 2 (NM_001082959/ENST00000339570), *SCARB1* variant 3 (NM_001367981/ENST00000415380), and *SCARB1* variant 4 (NM_001367982/ENST00000541205)—against the GRCh38.p13 primary assembly of the human genome. Diagram not drawn to scale, although the relative lengths of the exons have been maintained. (B) Upper panel, schematic representation of the predicted miR-125b-5p binding site on SCARB1 3′-UTR (bold and underlined) and the mutated SCARB1 3′-UTR with the deletion of eight nucleotides in the predicted miR-125b-5p binding site (strikethrough). Normalized luciferase activity 48 h after transfection of RAW264 cells that were co-transfected with pMirTarget vector containing the wild type 3′-UTR of SCARB-1 (p_SCARB1.WT) or the mutated 3′-UTR of SCARB-1 (p_SCARB1.Mut) in the 3′-UTR of the luciferase gene together with hsa-miR-125b-5p mimic. Luciferase values for the 3′-UTRs are normalized to the p_SCARB1 control plasmids (non-transfected miRNA mimic). The mean from the three replicates shows significant differences between the has-miR-125b-5p transfected wild type 3′-UTR SCARB1 plasmid and mutated 3′-UTR SCARB1 plasmid. The error bars represent the standard error of the mean (SEM). Significance was accepted at the level of $p < 0.05$, * compare to WT and & compare to Mutated. (C) Negative correlation between the expression of hsa-miRNA-125b (y-axis) and *SCARB1* (x-axis) in the arteries of the patients. Statistics: A Shapiro-Wilk normality test was performed to test for Gaussian distribution, and the differences between the groups were determined by an unpaired *t*-test. Pearson correlation (R) and the p-value were calculated for the C panel.

levels—whereas the ABCA1- and ABCG1-dependent pathways were upregulated [19,21],—we used cholesterol-unloaded macrophages. To the best of our knowledge, we showed for the first time that miR-125b overexpression reduced the macrophage and VSMC *SCARB1* mRNA and protein levels, leading to an impaired α-HDL-mediated macrophage cholesterol efflux *in vitro*. In contrast, we did not find significant alterations in the ABCG1 levels, and macrophage ABCA1 was very lowly expressed in these non-loaded-cholesterol macrophages. It should also be noted that the downregulation of both transporters in the non-cholesterol-loaded J774.1 mouse macrophages did not affect cholesterol efflux stimulated by HDL [19], thus highlighting the minor contribution of ABCA1/G1-dependent pathways in non-cholesterol-loaded macrophages. Furthermore, the miR-125b expression did not regulate the ABCA1-mediated efflux to lipid-free apoA-I in pCPT-cAMP-treated macrophages. In line with these findings, the rate of cholesterol efflux to mature α-HDL particles—but not

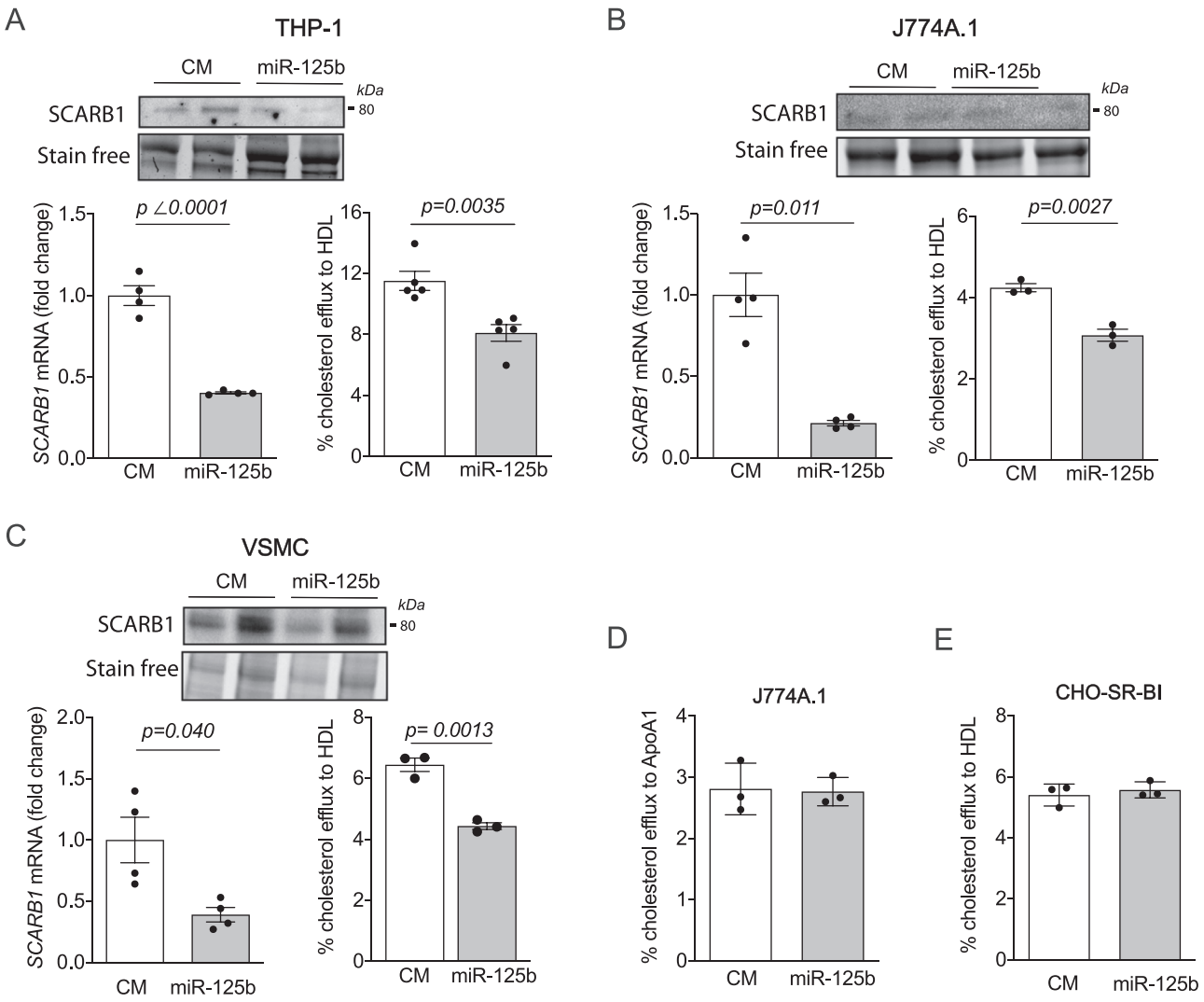

Fig. 3. miR-125b downregulates macrophage SR-B1 and impairs HDL-mediated macrophage cholesterol efflux. (A–C) Protein (upper panels) and qRT-PCR analysis (left) of *SCARB1* and cholesterol efflux (right) in (A) THP-1, (B) J774A.1, and (C) SMC cells transfected with CM or hsa-miR-125b. Western blot analysis of SCARB1 in the upper panels. The data normalization analysis was performed with stain free images. Representative experiment out of 2–3 experiments with similar results. qPCR data is presented as the mean ± SEM. Cholesterol efflux data is the mean ± SEM and representative of ≥ 2–3 experiments. Statistics: A Shapiro-Wilk normality test was performed for Gaussian distribution, and an unpaired *t*-test was performed to compare CM and miR-125b transfection. (D) Cholesterol efflux to ApoA1 from J774A.1 cells transfected with CM or miR-125b. (E) Cholesterol efflux to HDL from CHO cells expressing SCARB1 (CHO-SR-BI) transfected with CM or miR-125b. Data is the mean ± SEM and representative of ≥ 2–3 experiments in triplicate.

that to lipid-free apoA1—was significantly lower in the peritoneal macrophages isolated from SR-BI knockout mice [22,23]. Additionally, we also found that miR-125b-expressing mouse macrophages impaired the overall macrophage-specific RCT *in vivo* in WT mice fed a Western-type diet; this was mainly due to a defective HDL-mediated macrophage cholesterol efflux at all time points that were studied. However, cholesterol efflux to either human HDL3 or mouse whole serum was not affected in bone-marrow-derived macrophages from SR-B1-deficient mice and, consequently, neither *in vivo* macrophage RCT was altered [21]. In contrast with this latter study, we used WT mice fed a Western-type diet, which enhances both the diffusional component of macrophage cholesterol efflux and the whole macrophage-to feces RCT pathway [24]. Therefore, the relative importance of impaired SR-B1-mediated cholesterol efflux becomes quite apparent under conditions where the overall RCT pathway is stimulated, as also occurred with cholesterol efflux when the peritoneal macrophages of hyperlipidemic mice were defective for both SR-B1 and ABCA1 [23].

It should be noted that this *in vivo* RCT method was designed to evaluate the unidirectional transport of cholesterol from macrophages and it does not provide an assessment of cell cholesterol unloading or the cholesterol influx rate. However, we performed cholesterol influx experiments with radiolabel HDL *in vitro* and there were no differences between CM and miR-125b transfected cells. These *in vivo* models were mimicking a single—but significant—pathogenic aspect of HDL-mediated ATH. Indeed, the macrophage SR-B1 function within ATH has been reported to be highly dependent on the lipid context, indicating that cholesterol efflux may be more critical in advanced foam cell formation [3].

Overall, the results of our study support the concept that miRNA-125b downregulates SR-B1 in human and murine macrophages, as well as in VSMCs, thereby impairing macrophage cholesterol efflux *in vitro* and the whole macrophage-specific RCT pathway *in vivo*. These results also indicate a mechanism by which macrophage miR-125b may promote foam cell formation and ATH.

Interestingly, miR-125a, which belongs to the same miRNA family (and has an identical seed sequence) as miR-125b but has a different genomic location, is induced by oxLDL stimulation in monocyte/macrophages and inhibits lipid uptake and the inflammatory cytokine

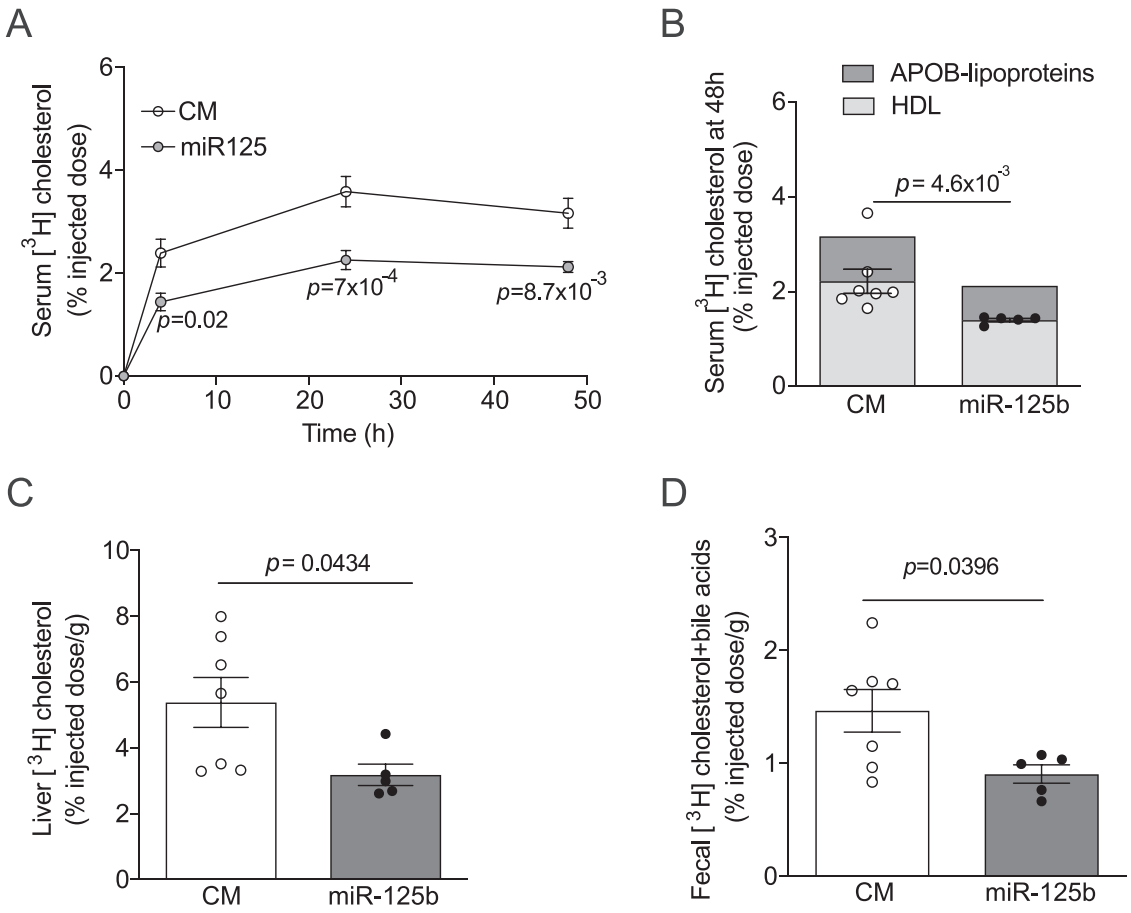

Fig. 4. miR-125b impairs HDL-mediated macrophage cholesterol efflux and macrophage-to-feces RCT *in vivo*. (A) Individually-housed wild-type mice were i.p. injected with [^{3}H]cholesterol-labeled mouse macrophages transfected with CM or hsa-miR-125, and serum [^{3}H]cholesterol was determined at the indicated times. (B) HDL- and APOB-lipoproteins-associated [^{3}H]cholesterol at 48 h (for clarity only, HDL-associated [^{3}H]cholesterol points are shown). (C) Hepatic [^{3}H]cholesterol at 48 h. (D) [^{3}H]cholesterol and [^{3}H]tracer from fecal bile acids of feces collected over 48 h. Values are expressed as the mean ± SEM of 7 and 5 wild-type mice injected with CM or hsa-miR-125 transfected [^{3}H]cholesterol-labeled mouse macrophages, respectively. The amount of [^{3}H]tracer was expressed as the fraction of the injected dose. Statistics: A Kolmogorov-Smirnov normality test was performed to test Gaussian distribution. (A-B) Repeated measures two-way ANOVA followed by a Bonferroni multiple-comparisons test was performed to compare the serum [^{3}H]cholesterol levels between the two groups in each time point and HDL- and APOB-lipoproteins-associated [^{3}H]cholesterol at 48 h. Two-way ANOVA results were: time, $p < 1 \times 10^{-4}$; and macrophage type, $p = 5.1 \times 10^{-3}$ and, at 48 h, lipoprotein distribution, $p < 1 \times 10^{-4}$; and macrophage type, $p = 0.0165$; APOB-lipoproteins-associated [^{3}H]cholesterol at 48 h were similar in both groups, $p = 0.6883$. (C-D) An unpaired *t*-test was performed to compare the liver and total fecal [^{3}H]cholesterol tracer (bile acids + cholesterol) between the two groups. Significance was accepted at the level of $p < 0.05$.

secretion, suggesting its potential role in ATH inflammatory responses [25]. Moreover, miR-125a and miR-125b have been also identified in VSMCs, as we confirmed in our patients, and has been suggested to play a role in vascular pathogenesis regulating vasoconstrictive gene expression and affecting the synthesis and secretion of many vasoactive substances [20]. Thus, future experiments will be needed to elucidate the role of miR-125a and miR-125b during the pathogenesis of ATH at the inflammatory and vascular level and shed lights onto the therapeutic potential of suppressing miR-125 *in vivo*.

CRediT authorship contribution statement

Miguel Hueso: Conceptualization, Methodology, Validation, Formal analysis, Investigation, Resources, Writing – review & editing, Funding aquisition. **Raquel Griñán:** Methodology, Validation, Formal analysis. **Adrián Mallen:** Methodology, Validation, Formal analysis. **Estanislao Navarro:** Conceptualization, Methodology, Validation, Formal analysis, Investigation. **Elvira Purqueras:** Methodology, Validation, Formal analysis. **Montse Gomá:** Methodology, Validation, Formal analysis. **Fabrizio Sbraga:** Resources. **Arnau Blasco-Lucas:** Resources. **Giovanna Revilla:** Methodology, Validation, Formal analysis. **David Santos:** Methodology, Validation. **Marina Canyelles:** Methodology, Validation. **Josep Julve:** Writing – review & editing. **Joan Carles Escolà-Gil:** Conceptualization, Methodology, Validation, Formal analysis, Investigation, Resources, Writing – original draft, Writing – review & editing. **Noemi Rotllan:** Conceptualization, Methodology, Validation, Formal analysis, Investigation, Resources, Writing – original draft, Writing – review & editing.

Author Contributions

MH, NR, and JC-E conceived and designed the study and wrote the manuscript. MH, RG, AM, EN, EP, MG, GR, DS, MC, JJ, JC-EG and NR performed experiments and analyzed data. FS and AB provided the aorta samples. All authors have read and agreed to the published version of the manuscript.

Funding

This work was funded by Ministerio de Ciencia, Innovación y Universidades (PID2019-104367RB-100), as well as from the Agencia Estatal de Investigación (AEI/10.13039/501100011033) within the

Subprograma Ramón y Cajal (RYC-201722879) to NR. This study has been funded by the Instituto de Salud Carlos III (Co-funded by the European Regional Development Fund (ERDF), a way to build Europe) through the project PI 18/01108 (to M.H), Rio Hortega contract CM20/00033 (to M.C) and Grant PI17/00232 (to JJ). This work was funded also by FEDER "Una manera de hacer Europa", and by Fundació La Marató de TV3 2016 (303/C/2016) (201602.30.31) (to JJ). JJ was recipient of a Miguel Servet Type 2 contract (CPII18/00004; ISCIII). CIBER de Diabetes y Enfermedades Metabólicas Asociadas (CIBERDEM) is a project of Instituto de Salud Carlos III. Institut de Recerca de l'Hospital de la Santa Creu i Sant Pau and Institut d'Investigació Biomèdica de Bellvitge-IDIBELL are accredited by the Generalitat de Catalunya as a Centre de Recerca de Catalunya (CERCA).

Declaration of Interest

All the authors declare that they do not have financial/personal interest or belief that could affect their objectivity.

Acknowledgments

We thank RICORS (RD21/0005/0001) and the CERCA Program/Generalitat de Catalunya for their institutional support. We want to particularly acknowledge the patients and the Biobank HUB-ICO-IDIBELL (PT17/0015/0024) integrated in the Spanish National Biobanks Network for their collaboration. We thank Benjamín Torrejón Escribano from the Advanced Light Microscopy Unit in the Scientific and Technical Facility for his help with the confocal images. We thank to Dr. Joerg Heere who kindly provide us with the CHO (Chinese-hamster ovary) cells.

Appendix A. Supporting information

Supplementary data associated with this article can be found in the online version at doi:10.1016/j.biopha.2021.112596.

References

[1] M.R.F. Linton, P.G. Yancey, S.S. Davies, W.G. Jerome, E.F. Linton, W.L. Song, A. C. Doran, K.C. Vickers, in: K.R. Feingold, B. Anawalt, A. Boyce, G. Chrousos, W. W. de Herder, K. Dhatariya, K. Dungan, A. Grossman, J.M. Hershman, J. Hofland, S. Kalra, G. Kaltsas, C. Koch, P. Kopp, M. Korbonits, C.S. Kovacs, W. Kuohung, B. Laferrere, E.A. McGee, R. McLachlan, J.E. Morley, M. New, J. Purnell, R. Sahay, F. Singer, C.A. Stratakis, D.L. Trence, D.P. Wilson (Eds.), The Role of Lipids and Lipoproteins in Atherosclerosis, Endotext South Dartmouth, MA, 2000.

[2] M.C. Phillips, Molecular mechanisms of cellular cholesterol efflux, J. Biol. Chem. 289 (2014) 24020–24029.

[3] M. Hoekstra, SR-BI as target in atherosclerosis and cardiovascular disease – a comprehensive appraisal of the cellular functions of SR-BI in physiology and disease, Atherosclerosis 258 (2017) 153–161.

[4] A. Braun, B.L. Trigatti, M.J. Post, K. Sato, M. Simons, J.M. Edelberg, R. D. Rosenberg, M. Schrenzel, M. Krieger, Loss of SR-BI expression leads to the early onset of occlusive atherosclerotic coronary artery disease, spontaneous myocardial infarctions, severe cardiac dysfunction, and premature death in apolipoprotein E-deficient mice, Circ. Res. 90 (2002) 270–276.

[5] S.N. Koenig, H.C. Sucharski, E.M. Jose, E.K. Dudley, F. Madiai, O. Cavus, A. D. Argall, J.L. Williams, N.P. Murphy, C.B.R. Keith, M. El Refaey, R.J. Gumina, K. D. Boudoulas, M.W. Milks, G. Sofowora, S.A. Smith, T.J. Hund, N.T. Wright, E. A. Bradley, K.M. Zareba, L.E. Wold, E.L. Mazzaferri Jr., P.J. Mohler, Inherited variants in SCARB1 cause severe early-onset coronary artery disease, Circ. Res. 129 (2021) 296–307.

[6] P. Zanoni, S.A. Khetarpal, D.B. Larach, W.F. Hancock-Cerutti, J.S. Millar, M. Cuchel, S. DerOhannessian, A. Kontush, P. Surendran, D. Saleheen, S. Trompet, J.W. Jukema, A. De Craen, P. Deloukas, N. Sattar, I. Ford, C. Packard, A. Majumder, D.S. Alam, E. Di Angelantonio, G. Abecasis, R. Chowdhury, J. Erdmann, B. G. Nordestgaard, S.F. Nielsen, A. Tybjaerg-Hansen, R.F. Schmidt, K. Kuulasmaa, D. J. Liu, M. Perola, S. Blankenberg, V. Salomaa, S. Mannisto, P. Amouyel, D. Arveiler, J. Ferrieres, M. Muller-Nurasyid, M. Ferrario, F. Kee, C.J. Willer, N. Samani, H. Schunkert, A.S. Butterworth, J.M. Packard, G.M. Peloso, N.O. Stitziel, J. Danesh, S. Kathiresan, D.J. Rader, C.H.D.E. Consortium, C.A.E. Consortium, C. Global Lipids Genetics, Rare variant in scavenger receptor BI raises HDL cholesterol and increases risk of coronary heart disease, Science 351 (2016) 1166–1171.

[7] A. Helgadottir, P. Sulem, G. Thorgeirsson, S. Gretarsdottir, G. Thorleifsson, B. O. Jensson, G.A. Arnadottir, I. Olafsson, G.I. Eyjolfsson, O. Sigurdardottir, U. Thorsteinsdottir, D.F. Gudbjartsson, H. Holm, K. Stefansson, Rare SCARB1 mutations associate with high-density lipoprotein cholesterol but not with coronary artery disease, Eur. Heart J. 39 (2018) 2172–2178.

[8] D.A. Chistiakov, A.A. Melnichenko, V.A. Myasoedova, A.V. Grechko, A.N. Orekhov, Mechanisms of foam cell formation in atherosclerosis, J. Mol. Med. 95 (2017) 1153–1165.

[9] K.H. Lao, L. Zeng, Q. Xu, Endothelial and smooth muscle cell transformation in atherosclerosis, Curr. Opin. Lipidol. 26 (2015) 449–456.

[10] M. Hueso, L. De Ramon, E. Navarro, E. Ripoll, J.M. Cruzado, J.M. Grinyo, J. Torras, Silencing of CD40 in vivo reduces progression of experimental atherogenesis through an NF-kappaB/miR-125b axis and reveals new potential mediators in the pathogenesis of atherosclerosis, Atherosclerosis 255 (2016) 80–89.

[11] T. Huan, J. Rong, C. Liu, X. Zhang, K. Tanriverdi, R. Joehanes, B.H. Chen, J. M. Murabito, C. Yao, P. Courchesne, P.J. Munson, C.J. O'Donnell, N. Cox, A. D. Johnson, M.G. Larson, D. Levy, J.E. Freedman, Genome-wide identification of microRNA expression quantitative trait loci, Nat. Commun. 6 (2015) 6601.

[12] Z. Hu, W.J. Shen, F.B. Kraemer, S. Azhar, MicroRNAs 125a and 455 repress lipoprotein-supported steroidogenesis by targeting scavenger receptor class B type I in steroidogenic cells, Mol. Cell Biol. 32 (2012) 5035–5045.

[13] K. Hirano, S. Yamashita, Y. Nakagawa, T. Ohya, F. Matsuura, K. Tsukamoto, Y. Okamoto, A. Matsuyama, K. Matsumoto, J. Miyagawa, Y. Matsuzawa, Expression of human scavenger receptor class B type I in cultured human monocyte-derived macrophages and atherosclerotic lesions, Circ. Res. 85 (1999) 108–116.

[14] A. Casas, A. Mallen, A. Blasco-Lucas, F. Sbraga, J. Guiteras, N. Bolanos, E. Castano, J. Torras, J.M. Cruzado, E. Navarro, M. Hueso, Chronic kidney disease-associated inflammation increases the risks of acute kidney injury and mortality after cardiac surgery, Int. J. Mol. Sci. 21 (2020) 9689.

[15] I. Bar, A. Merhi, F. Abdel-Sater, A. Ben Addi, S. Sollennita, J.L. Canon, P. Delree, The microRNA miR-210 is expressed by cancer cells but also by the tumor microenvironment in triple-negative breast cancer, J. Histochem. Cytochem. 65 (2017) 335–346.

[16] L. Goedeke, N. Rotllan, A. Canfran-Duque, J.F. Aranda, C.M. Ramirez, E. Araldi, C. S. Lin, N.N. Anderson, A. Wagschal, R. de Cabo, J.D. Horton, M.A. Lasuncion, A. M. Naar, Y. Suarez, C. Fernandez-Hernando, MicroRNA-148a regulates LDL receptor and ABCA1 expression to control circulating lipoprotein levels, Nat. Med. 21 (2015) 1280–1289.

[17] J.C. Escola-Gil, M. Lee-Rueckert, D. Santos, L. Cedo, F. Blanco-Vaca, J. Julve, Quantification of in vitro macrophage cholesterol efflux and in vivo macrophage-specific reverse cholesterol transport, Methods Mol. Biol. 1339 (2015) 211–233.

[18] L. Cedo, S. Fernandez-Castillejo, L. Rubio, J. Metso, D. Santos, D. Munoz-Aguayo, A. Rivas-Urbina, M. Tondo, K.A. Mendez-Lara, M. Farras, M. Jauhiainen, M. J. Motilva, M. Fito, F. Blanco-Vaca, R. Sola, J.C. Escola-Gil, Phenol-enriched virgin olive oil promotes macrophage-specific reverse cholesterol transport in vivo, Biomedicines 8 (2020) 266.

[19] L. Cedo, J. Metso, D. Santos, A. Garcia-Leon, N. Plana, S. Sabate-Soler, N. Rotllan, A. Rivas-Urbina, K.A. Mendez-Lara, M. Tondo, J. Girona, J. Julve, V. Pallares, A. Benitez-Amaro, V. Llorente-Cortes, A. Perez, D. Gomez-Coronado, A. K. Ruotsalainen, A.L. Levonen, J.L. Sanchez-Quesada, L. Masana, P.T. Kovanen, M. Jauhiainen, M. Lee-Rueckert, F. Blanco-Vaca, J.C. Escola-Gil, LDL receptor regulates the reverse transport of macrophage-derived unesterified cholesterol via concerted action of the HDL-LDL axis: insight from mouse models, Circ. Res. 127 (2020) 778–792.

[20] D. Li, P. Yang, Q. Xiong, X. Song, X. Yang, L. Liu, W. Yuan, Y.C. Rui, MicroRNA-125a/b-5p inhibits endothelin-1 expression in vascular endothelial cells, J. Hypertens. 28 (2010) 1646–1654.

[21] X. Wang, H.L. Collins, M. Ranalletta, I.V. Fuki, J.T. Billheimer, G.H. Rothblat, A. R. Tall, D.J. Rader, Macrophage ABCA1 and ABCG1, but not SR-BI, promote macrophage reverse cholesterol transport in vivo, J. Clin. Invest. 117 (2007) 2216–2224.

[22] M. Van Eck, I.S. Bos, R.B. Hildebrand, B.T. Van Rij, T.J. Van Berkel, Dual role for scavenger receptor class B, type I on bone marrow-derived cells in atherosclerotic lesion development, Am. J. Pathol. 165 (2004) 785–794.

[23] Y. Zhao, M. Pennings, R.B. Hildebrand, D. Ye, L. Calpe-Berdiel, R. Out, M. Kjerrulf, E. Hurt-Camejo, A.K. Groen, M. Hoekstra, W. Jessup, G. Chimini, T.J. Van Berkel, Van, Eck M. Enhanced foam cell formation, atherosclerotic lesion development, and inflammation by combined deletion of ABCA1 and SR-BI in bone marrow-derived cells in LDL receptor knockout mice on western-type diet, Circ. Res. 107 (2010) e20–31.

[24] J.C. Escola-Gil, G. Llaverias, J. Julve, M. Jauhiainen, J. Mendez-Gonzalez, F. Blanco-Vaca, The cholesterol content of Western diets plays a major role in the paradoxical increase in high-density lipoprotein cholesterol and upregulates the macrophage reverse cholesterol transport pathway, Arterioscler. Thromb. Vasc. Biol. 31 (2011) 2493–2499.

[25] T. Chen, Z. Huang, L. Wang, Y. Wang, F. Wu, S. Meng, C. Wang, MicroRNA-125a-5p partly regulates the inflammatory response, lipid uptake, and ORP9 expression in oxLDL-stimulated monocyte/macrophages, Cardiovasc. Res. 83 (2009) 131–139.